J Neurol
DOI 10.1007/s00415-014-7440-6

ORIGINAL COMMUNICATION

A novel computerized algorithm to detect microstructural brainstem pathology in Parkinson's disease using standard 3 Tesla MR imaging

Kai Boelmans · Lothar Spies · Jan Sedlacik · Jens Fiehler · Holger Jahn · Christian Gerloff · Alexander Münchau

Received: 23 March 2014 / Revised: 10 July 2014 / Accepted: 11 July 2014

Abstract Increased deposition of α-synuclein in Parkinson's disease (PD) is known to be prominent in the brainstem and discussed to be clinically relevant for motor and non-motor features. Whether structural magnetic resonance imaging is capable to detect degraded tissue microstructure caused by increased deposition of α-synuclein at this predilection site in PD remains unclear. We hypothesize that microstructural degradation in the brainstem leads to a reduced T1 contrast provoking standard tissue segmentation engines to misclassify tissue as additional grey matter in regions predominantly composed of white matter. High-resolution T1-weighted three-dimensional magnetization prepared rapid gradient echo (MPRAGE) imaging at 3 Tesla in fifty-two PD patients with mild-to-moderate disease severity and in forty age- and gender-matched healthy controls was performed. A dedicated computerized algorithm that comprises standard tissue segmentation in combination with a statistical test was set up that evaluates grey matter composition on voxel level. The algorithm detected a single significant cluster of voxels with enhanced grey matter (cluster volume is 1,368 mm^3, $p < 0.05$ corrected for false discovery rate) in the pontomedullary junction of the brainstem in PD patients as compared to healthy controls. Furthermore, absolute grey matter volume was significantly higher in the brainstem of the PD group compared to healthy controls. We conclude that this cluster may reflect α-synuclein induced microstructural brainstem pathology in PD.

Keywords Parkinson's disease · Pontomedullary junction · T1-weighted magnetic resonance imaging · Brain tissue segmentation

K. Boelmans (✉) · H. Jahn
Department of Psychiatry, Memory Clinic, University Medical Center Hamburg-Eppendorf, Martinistrasse 52, 20246 Hamburg, Germany
e-mail: k.boelmans@uke.uni-hamburg.de

L. Spies
jung diagnostics GmbH, Hamburg, Germany

J. Sedlacik · J. Fiehler
Department of Neuroradiology, University Medical Center Hamburg-Eppendorf, Hamburg, Germany

C. Gerloff
Department of Neurology, University Medical Center Hamburg-Eppendorf, Hamburg, Germany

A. Münchau
Department of Paediatric and Adult Movement Disorders and Neuropsychiatry, Institute of Neurogenetics, University of Lübeck, Lübeck, Germany

Introduction

Classical Parkinson's disease (PD) is a progressive neurodegenerative disorder defined by bradykinesia, rigidity, rest tremor, and postural instability in advanced stages. Recently, the clinical spectrum of PD has been expanded to comprise non-motor symptoms including hyposmia, pain, mood disorders such as anxiety or depression, and sleep disturbances like rapid-eye-movement behavior disorder [1]. These non-motor features often precede motor symptoms and might, therefore, be indicative of early disease or valuable for identifying at risk patients. Several of these motor and non-motor features such as dyskinesias [2], depression [3] or pain [4] are related to pathology in the pontomedullary junction where α-synuclein aggregates in PD [5, 6].

To date no reliable imaging markers for structural brainstem pathology in PD based on standard magnetic

Published online: 26 July 2014

resonance (MR) imaging exist [7]. One reason for this is that brainstem imaging is challenging due to distortions in the magnetic field caused by neighboring air cavities and pulsatile motion of the brain related to the cardiac and respiratory cycle. Another reason is that intraneuronal α-synuclein-based Lewy body inclusions are currently not detectable using high-field or non-contrast-enhanced MR imaging [8]. This notwithstanding, growing evidence suggests a relationship between MR signal changes and cellular brainstem pathology in PD. Using T1-weighted neuromelanin MR imaging, for example, a reduced signal intensity in the locus coeruleus was demonstrated in late PD patients [9]. Signal reduction directly correlated with the amout of neuromelanin-containing neurons in autopsied brains [10].

The first study demonstrating in vivo that conventional T1-weighted MR imaging is able to detect white matter (WM) atrophy in the pontomedullary junction in mild-to-moderate PD was performed by Jubault and colleagues using voxel-based morphometry [11].

We hypothesize that tissue with high α-synuclein load is expected to appear slightly darker than the surrounding WM in T1-weighted MR images because α-synuclein accumulation causes a cascade of multiple intracellular and potentially extracellular pathogenetic effects including mitochondrial, lysosomal and synaptic dysfunctions [12]. These effects which commonly result in neuronal death are subsumed as α-synuclein induced microstructural degradation [5]. Microstructural tissue degradation induces prolonged T1 relaxation times translating into a darker appearance of WM. We refer to the altered tissue property as 'reduced WM contrast' (RWC) in T1-weighted images. RWC might be difficult to detect by visual inspection, but can potentially be accessed using fully automated image analyses. If a segmentation engine is applied which is designed to classify normal tissue, RWC regions are expected to be partially misclassified as grey matter (GM). In our approach this misclassification is not considered as a defect of the segmentation algorithm, but rather a facilitator to determine the lesion size. Hence no attempt was made to correct for this misclassification. A recent publication demonstrated that T1-hypointense multiple sclerosis lesions can be detected using the same principle [13].

The aim of the present study was to explore the feasibility and accuracy of standard T1-weighted MR imaging equipped with a novel computerized algorithm to detect microstructural brainstem pathology in PD.

Patients and methods

Participants

Sixty-eight inpatients with classical PD according to the United Kingdom (UK) PD Brain Bank criteria were consecutively enrolled and examined by movement disorders specialists. We excluded patients with cerebrovascular disorders, a history of traumatic brain injury, dementia (Mini-Mental State Examination (MMSE) score <23) or other neurologic or systemic diseases. Fifty-two PD patients [mean age 65.3 ± 8.9 (40–77) years] fulfilled inclusion/exclusion criteria. The Unified PD Rating Scale (UPDRS) was performed in the 'on' and 'off' condition [14]. For the off condition, L-dopa was withdrawn at least 12 h before scoring. Long-acting dopamine agonists were replaced by L-dopa equivalent doses 3–5 days prior to clinical testing. The modified Hoehn and Yahr score was used to assess PD related disease severity [15].

A normative database was assembled comprising forty healthy controls [mean age 62.5 ± 11.6 (41–86) years]. Each eligible control subject was thoroughly examined by an experienced neurologist to ensure that no asymptomatic PD patient was included.

Image acquisition

Images of PD patients and healthy controls were acquired with a 3 Tesla MR scanner (Siemens Skyra) using a standard MR protocol. The protocol comprises a high-resolution three-dimensional T1-weighted MPRAGE imaging sequence providing enhanced tissue contrast. The following settings were used: TR = 1,900 ms, TE = 2.46 ms, TI = 900 ms, flip angle = 9°. Slice thickness was 0.94 mm and pixel size was 0.94 mm for both directions.

Image processing pipeline

The algorithm comprises a standard tissue segmentation engine in combination with a voxelwise statistical test that detects disproportions of tissue in regions predominantly composed of WM.

Tissue segmentation

MR images were segmented and stereotactically normalized to the Montreal Neurological Institute (MNI) space using the combined segmentation and registration approach implemented in the SPM8 software package (release April 2009; Wellcome Trust Centre for Neuroimaging, London, UK). Prior tissue probability maps for GM, WM and cerebrospinal fluid (CSF) were deployed to assist segmentation and registration, which were generated from a population of 662 healthy elderly subjects [16]. Maps feature an isotropic resolution of 1 mm approximately matching the resolution of the images to be segmented.

For all analyses, we used the default settings of the unified segmentation engine: A mixture of Gaussians to

model intensity distributions of GM, WM, CSF and '1–GM–WM–CSF' was deployed. The number of Gaussians was 2, 2, 2, and 4, respectively. Further parameters were: 25 mm for the cutoff of three-dimensional discrete cosine transform basis function for spatial warping, very light regularization (0.0001), and 60 mm width for the Gaussian smoothness of the intensity bias field. The unified segmentation approach yielded three stereotactically normalized tissue maps (GM, WM, and CSF) with a voxel volume of 1 mm^3 and intensities between 0 and 1. The determinant of the Jacobian of the transformation field was applied locally to ensure that the volume was preserved after stereotactical normalization. The tissue maps were further processed by applying a CSF mask to compensate for misclassification at the interface between CSF and bone [17]. Total GM, WM and CSF volumes were estimated by summation of all voxel values of the respective tissue map multiplied by the voxel volume, representing the total intracranial volume (TIV).

Voxelwise statistical test

For RWC detection a voxelwise statistical test was configured to test GM enhancement in regions that are predominantly composed of WM. These regions are defined by voxels of a prior tissue probability map [16], for which WM probability is equal or greater than 0.5. A respective binary mask, denoted subsequently as WM mask, was derived which renders one for a voxel belonging to this voxel set. All other voxels of the mask were set to zero. Voxelwise statistical tests were performed on stereotactically normalized GM tissue maps restricted to voxels belonging to the WM mask with an isotropic voxel grid with grid size of 2 mm. The voxel volume was 0.008 ml. Voxelwise statistical tests produced parametric maps with the same dimension and voxel volume.

We applied a one-sided two sample t test including age and TIV as covariates to test for GM enhancements in the PD group as opposed to the normative database of healthy controls. Gender is not included since TIV eliminates sex differences [18]. Prior to testing, GM tissue maps of both groups were further aligned using a high-dimensional elastic registration technique (DARTEL) [19]. Then, each GM tissue map was smoothed by an isotropic Gaussian filter with a full width at half maximum of 4 mm which is considered as sufficient in combination with DARTEL [18]. The test was restricted to voxels defined by the WM mask. The cluster threshold was set to zero. Results were considered significant for $p \leq 0.05$, corrected for multiple comparisons using the false discovery rate (FDR) method [20]. The generation of the resulting parametric map is illustrated in Fig. 1.

Calculation of effect size

The 'effect size' for a PD patient or a healthy control was estimated by calculating the total GM volume across WM dominating regions of the brainstem (brainstem GM volume). The brainstem was delineated by a binary mask derived from a probabilistic whole-brain atlas in MNI space as described by Shattuck et al. [21]. Voxels of the stereotactically normalized GM tissue map, which are within the binary mask and for which the corresponding voxels of the WM template feature WM ≥ 0.5, were included (the total volume of all included voxels was 28,400 mm^3).

Statistical analysis

Differences in age between PD patients and controls were analyzed using the Mann–Whitney U test because of unequal variances; differences in TIV were analyzed using a two-sided t test. Gender distribution between both groups was analyzed with Pearson's χ^2 tests. For a comparison of the effect size between PD patients and healthy controls, one-sided t test was used. Correlations of brainstem GM volumes with disease duration and UPDRS-III (off condition) were calculated by Pearson's correlation coefficient. The statistical threshold was set to $p \leq 0.05$.

Results

Participants

Participant and clinical characteristics are summarized in Table 1. There were no significant differences in baseline parameters between PD patients and healthy controls (Table 1).

Group analysis

The group wise comparison of GM tissue images of PD patients and the normative database of healthy controls yielded a single symmetrical cluster of RWC in the PD group in the pontomedullary junction of the brainstem (Fig. 2). The cluster was found to be significant on cluster level ($p < 0.003$ FDR corrected), but not on peak level ($p = 0.154$ FDR corrected). The volume of the cluster was 1,368 mm^3, the MNI coordinates of the hot spot (t score = 4.29) were (2; −30; −46). No other significant cluster was found.

Effect size

We found that brainstem GM volume was significantly higher in the PD group (mean 2,006 ± 682 mm^3) compared

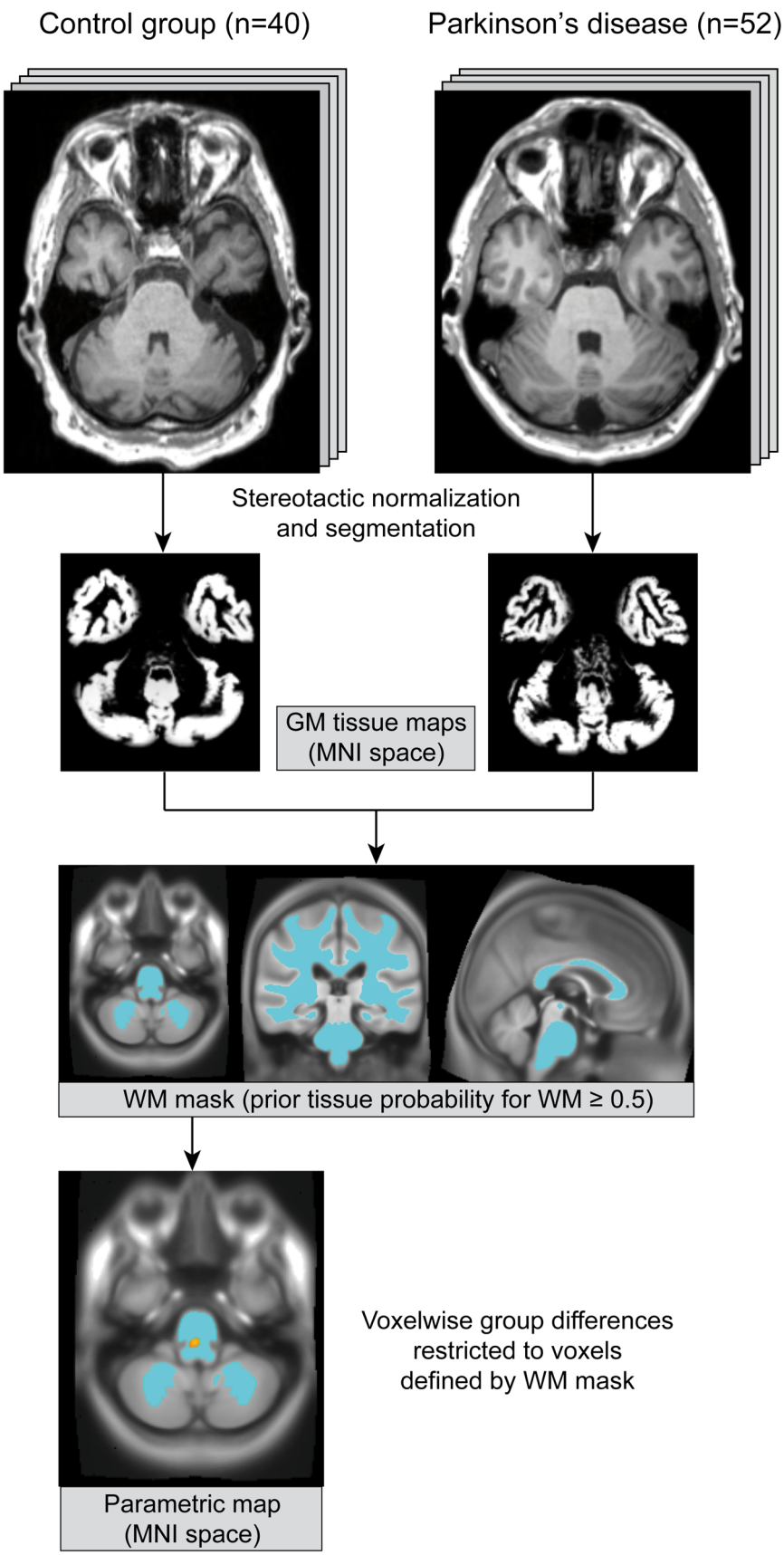

Fig. 1 Flowchart of the image processing pipeline. Two-step analysis of tissue segmentation and voxelwise statistical tests to detect reduced white matter contrast. The turquoise surface illustrates the area that is 'dominated' by white matter (regions with white matter ≥ 0.5 derived from prior tissue probability maps)

Table 1 Participant and clinical characteristics

	Parkinson's disease patients ($n = 52$)	Healthy controls ($n = 40$)
Age at examination, year, mean ± SD (range)[a]	65.3 ± 8.9 (40–77)	62.5 ± 11.6 (41–86)*
Gender, M/F[b]	35/17	26/14[†]
Handedness, R/L	50/2	39/1
Total intracranial volume, ml, mean ± SD (range)[c]	1,433 ± 157	1,424 ± 113[§]
Disease duration, year, mean ± SD (range)	11.6 ± 6.6 (0.5–30.2)	NA
Age at disease onset, year, mean ± SD (range)	53.7 ± 9.8 (27.5–75.2)	NA
First affected body side, R/L	23/29	NA
Subtype at disease onset, TD, AR, MX	18, 17, 17	NA
Subtype at examination, TD, AR, MX	17, 31, 4	NA
Hoehn and Yahr, mean ± SD (range)	2.6 ± 0.8 (1–4)	NA
UPDRS motor score (OFF condition), mean ± SD (range)	36.8 ± 13.0 (14–63)	NA
UPDRS motor score (ON condition), mean ± SD (range)	20.8 ± 10.2 (5–52)	NA
MMSE, mean ± SD (range)	27.4 ± 2.0 (23–30)	NA

AR akinetic-rigid subtype, *MMSE* Mini-Mental State Examination, *MX* mixed subtype, *NA* not applicable, *UPDRS* Unified Parkinson's Disease Rating Scale, *TD* tremor-dominant subtype, *SD* standard deviation

* $P = 0.267$, † $P = 0.816$, § $P = 0.755$

[a] Mann–Whitney *U* test, [b] Pearson's χ^2 test, [c]two-tailed *t* test

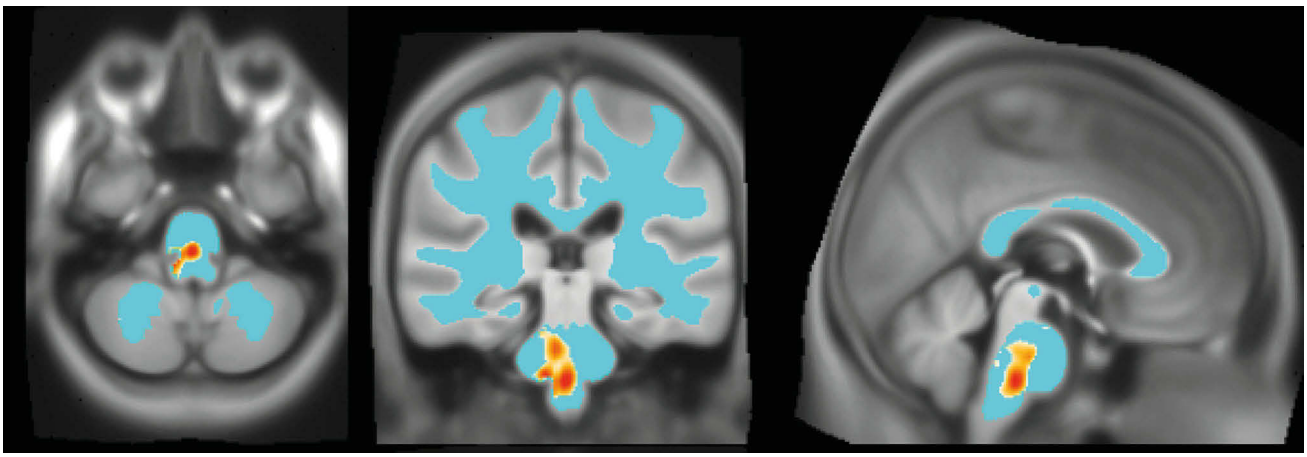

Fig. 2 Cluster topography. Spatial localization of the cluster of reduced white matter contrast in Parkinson's disease compared to the control group. The cluster of significance is located in the pontomedullary brainstem area ($p < 0.003$, FDR corrected, no extend threshold). MNI coordinates of the hot spot (*t* score = 4.29) were (2, −30, −46)

to healthy controls (mean 1,715 ± 624 mm^3) ($p = 0.019$, adjusted for age) (Fig. 3). Brainstem GM volume of healthy controls correlated with age but not with TIV. Hence brainstem GM volumes were only adjusted for age. No clinico-imaging correlations were found between brainstem GM volume and disease duration ($r = 0.023$, $p = 0.871$) and UPDRS-III ($r = 0.008$, $p = 0.955$), respectively.

Discussion

The present study investigated whether microstructural brainstem degradation in PD can be characterized using standard 3 Tesla MR imaging as used in clinical routine. The proposed method detected a single significant cluster of RWC in the brainstem in PD patients compared to healthy controls, anatomically matching the pontine tegmentum and rostral part of the medulla oblongata. These regions are topographically congruent to the histopathologically determined lesion pattern in PD patients proposed by Braak and colleagues [6, 22]. The pontomedullary area encompasses parts of the lower raphe nuclei, reticular formation and coeruleus–subcoeruleus complex, which are engaged in serotonergic, dopaminergic and noradrenergic transmissions. Dysregulations in these areas are relevant for a spectrum of PD motor symptoms including dyskinesias [2] and gait disturbance [23], but also for non-motor features such as depression [3] and pain [4].

Conventional and advanced MR studies have recently reported an involvement of the pontomedullary brainstem in PD [11, 24, 25], but also in other α-synuclein pathologies such as dementia with Lewy bodies or idiopathic

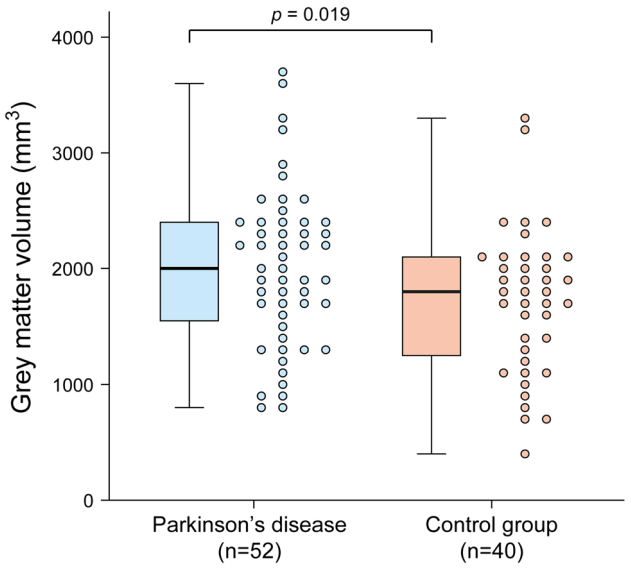

Fig. 3 Effect size. *Box* and *dotplots* of grey matter volume in the brainstem evaluated for white matter dominating regions (white matter probability ≥0.5) for Parkinson's disease patients (*blue*) and healthy controls (*pink*). The *bottom* and *top* of the *box* represent the 25–75 % percentile. The *bold black line* represents the median (50 % percentile). Whiskers *under* and *above* the boxes characterize the minimum and maximum data values

rapid-eye-movement sleep disorder [26]. Jubault and colleagues [11] described a comparable pattern of brainstem abnormalities in 23 PD patients at Hoehn and Yahr stages I–II compared to healthy controls in a group level analysis that corresponds very closely to our results (peak significance in MNI space: −1, −36, −49; volume 4,287 mm^3). They identified a WM volume reduction in their primary analysis, which indirectly confirms our analysis since a reduction of WM is normally accompanied by a relative increase in GM due to volume preservation. However, an associated WM reduction could not be replicated in our study, possibly due to pronounced WM variations of the normative database. Similarly, Scherfler et al. [26] did not find WM atrophy in the pontomesencephalic tegmentum in α-synuclein mediated idiopathic rapid-eye-movement sleep disorder.

An involvement of non-dopaminergic nuclei of the midbrain and of the pontine reticular formation in early PD patients (disease duration 4.0 ± 2.3 years) was also mapped by WM decrease in T1 intensities, affecting the level of the pontomesencephalic junction [25]. Using a novel MR method based on adiabatic $R1_\rho$ and modified magnetization transfer mapping, Tuite et al. [27] analyzed a 4-mm paramedian brainstem slice and showed that the medullary parts of the raphe complex are more affected than the rostral parts in nine PD patients compared to ten healthy controls. Characterizing the neurochemical correlates of the pontomedullary damage in mild-to-moderate PD, 7T ^{1}H-MR spectroscopy implies alterations of GABAergic transmission in these areas, which may represent a biomarker for disease staging in the future [24].

Following our hypothesis, RWC might reflect a subtle degenerative process in brainstem tissue triggered by the extensive accumulation of α-synuclein-immunoreactive Lewy bodies, which are hallmarks of PD pathology [5]. The overexpression of α-synuclein clearly results in neuronal death mediated by different pathways (e.g. macroautophagy, autophagy of mitochondria, and axonal and synaptic structural alterations) [12]. However, as a limitation, to date no published work exists demonstrating a direct relationship between α-synuclein load and consecutive tissue alterations compared to T1 signal intensity, including studies from animal and phantom imaging. Although the novel approach seems to be particularly sensitive to detect α-synuclein induced microstructural pathology, direct evidence for this conjecture is lacking. A comparison between in vivo and post mortem MR microscopy in PD brains may be one strategy to overcome this challenge.

The computerized algorithm in this study deploys voxel-based morphometry using a non-standard configuration: Following a standard tissue segmentation engine, the statistical test to detect RWC was restricted to voxels containing a minimum of 50 % WM extracted from a population based WM atlas [16]. The design was originally developed for the detection of T1-hypointense multiple sclerosis lesions in deep WM regions (e.g. voxels with a minimum of 85 % WM in an average population) [13]. By accepting voxels with 50 % or more WM content, i.e. dominance of WM, a large part of the brainstem is searched by the algorithm. It has to be explained that GM microstructures such as brainstem nuclei are assumed to be smaller than a voxel (8 mm^3 voxel volume) and may thus be masked by partial volume effects in WM dominating areas. On an individual level, α-synuclein accumulation and consecutive cellular pathology prolong T1 relaxation times leading to RWC. Technically, the algorithm interprets RWC as 'additional' GM and 'less' WM and subsequently compares GM content between two groups. From the pathophysiological point of view, RWC in the brainstem most probably represents an identifiable imaging marker connected to α-synuclein pathology. Whether RWC is caused by α-synuclein accumulation isolated in brainstem nuclei or by surrounding WM tissue in terms of an α-synuclein propagation can not be resolved with the current setup.

The degree of brainstem pathology, however, is independent from global clinical scores such as disease duration or severity of motor disability, which is in line with former studies [11]. According to the negative clinico-imaging correlations, the lesion pattern might be

interpreted as a pure on–off criterion. However, it has to be considered that PD is a heterogeneous disease and many patients may not follow the classical PD staging scheme proposed by Braak (Braak hypothesis). In a neuropathologically verified UK cohort (Cambridgeshire and Nottingham) only 51 % corresponded to the Braak hypothesis, whereas a high proportion of cases showed a distribution of α-synuclein pathology predominantly affecting the amygdala (29 %) or the cortex, but not the lower brainstem (17 %) [28]. Comparable results from the UK PD Society Tissue Bank demonstrated α-synuclein pathology predominantly affecting the substania nigra and nucleus basalis of Meynert, but did not support the existence of a medullary induction site in PD. In detail, 47 % of the PD patients did not fulfill the predicted rostral-to-caudal spread of α-synuclein pathology [29]. On the other hand, there are also reports of advanced stages of α-synuclein pathology in the brainstem without parkinsonism [30]. Thus, the staging scheme is not consistent in all PD courses [31].

In conclusion, data presented here suggest that microstructural degradation in the pontomedullary brainstem can be detected by a novel computerized algorithm using standard 3 Tesla MR imaging as commonly deployed in clinical routine. Prospective studies are required to validate the presented brainstem marker, particularly in prodromal PD stages and in other α-synuclein pathologies such as dementia with Lewy bodies.

Acknowledgments We like to thank Dr. Ralph Buchert for a careful revision of the manuscript. Support by the Deutsche Forschungsgemeinschaft (SFB 936) is gratefully acknowledged.

Conflicts of interest The authors declare that they have no conflict of interest.

Ethical standards The study protocol was approved by the ethics committee of the Ärztekammer Hamburg, Germany, and all subjects gave written informed consent for study participation consistent with the Declaration of Helsinki.

References

1. Gallagher DA, Lees AJ, Schrag A (2010) What are the most important nonmotor symptoms in patients with Parkinson's disease and are we missing them? Mov Disord 25:2493–2500
2. Cheshire PA, Williams DR (2012) Serotonergic involvement in levodopa-induced dyskinesias in Parkinson's disease. J Clin Neurosci 19:343–348
3. Politis M, Wu K, Loane C, Turkheimer FE, Molloy S, Brooks DJ, Piccini P (2010) Depressive symptoms in PD correlate with higher 5-HTT binding in raphe and limbic structures. Neurology 75:1920–1927
4. Grinberg LT, Rueb U, Alho AT, Heinsen H (2010) Brainstem pathology and non-motor symptoms in PD. J Neurol Sci 289:81–88
5. Del Tredici K, Braak H (2012) Lewy pathology and neurodegeneration in premotor Parkinson's disease. Mov Disord 27:597–607
6. Braak H, Ghebremedhin E, Rub U, Bratzke H, Del Tredici K (2004) Stages in the development of Parkinson's disease-related pathology. Cell Tissue Res 318:121–134
7. Marek K, Jennings D (2009) Can we image premotor Parkinson disease? Neurology 72:S21–S26
8. Vernon AC, Ballard C, Modo M (2010) Neuroimaging for Lewy body disease: is the in vivo molecular imaging of alpha-synuclein neuropathology required and feasible? Brain Res Rev 65:28–55
9. Miyoshi F, Ogawa T, Kitao SI, Kitayama M, Shinohara Y, Takasugi M, Fujii S, Kaminou T (2013) Evaluation of Parkinson disease and Alzheimer disease with the use of neuromelanin MR imaging and (123)I-metaiodobenzylguanidine scintigraphy. AJNR Am J Neuroradiol 34:2113–2118
10. Kitao S, Matsusue E, Fujii S, Miyoshi F, Kaminou T, Kato S, Ito H, Ogawa T (2013) Correlation between pathology and neuromelanin MR imaging in Parkinson's disease and dementia with Lewy bodies. Neuroradiology 55:947–953
11. Jubault T, Brambati SM, Degroot C, Kullmann B, Strafella AP, Lafontaine AL, Chouinard S, Monchi O (2009) Regional brain stem atrophy in idiopathic Parkinson's disease detected by anatomical MRI. PLoS One 4:e8247
12. Vekrellis K, Xilouri M, Emmanouilidou E, Rideout HJ, Stefanis L (2011) Pathological roles of alpha-synuclein in neurological disorders. Lancet Neurol 10:1015–1025
13. Spies L, Tewes A, Suppa P, Opfer R, Buchert R, Winkler G, Raji A (2013) Fully automatic detection of deep white matter T1 hypointense lesions in multiple sclerosis. Phys Med Biol 58:8323–8337
14. Goetz CG, Tilley BC, Shaftman SR, Stebbins GT, Fahn S, Martinez-Martin P, Poewe W, Sampaio C, Stern MB, Dodel R, Dubois B, Holloway R, Jankovic J, Kulisevsky J, Lang AE, Lees A, Leurgans S, LeWitt PA, Nyenhuis D, Olanow CW, Rascol O, Schrag A, Teresi JA, van Hilten JJ, LaPelle N, Movement Disorder Society URTF (2008) Movement Disorder Society-sponsored revision of the Unified Parkinson's Disease Rating Scale (MDS-UPDRS): scale presentation and clinimetric testing results. Mov Disord 23:2129–2170
15. Hoehn MM, Yahr MD (1967) Parkinsonism: onset, progression and mortality. Neurology 17:427–442
16. Lemaitre H, Crivello F, Grassiot B, Alperovitch A, Tzourio C, Mazoyer B (2005) Age- and sex-related effects on the neuroanatomy of healthy elderly. Neuroimage 26:900–911
17. Huppertz HJ, Kroll-Seger J, Kloppel S, Ganz RE, Kassubek J (2010) Intra- and interscanner variability of automated voxel-based volumetry based on a 3D probabilistic atlas of human cerebral structures. Neuroimage 49:2216–2224
18. Henley SM, Ridgway GR, Scahill RI, Kloppel S, Tabrizi SJ, Fox NC, Kassubek J, Group EIW (2010) Pitfalls in the use of voxel-based morphometry as a biomarker: examples from huntington disease. AJNR Am J Neuroradiol 31:711–719
19. Ashburner J (2007) A fast diffeomorphic image registration algorithm. Neuroimage 38:95–113
20. Chumbley JR, Friston KJ (2009) False discovery rate revisited: FDR and topological inference using Gaussian random fields. Neuroimage 44:62–70
21. Shattuck DW, Mirza M, Adisetiyo V, Hojatkashani C, Salamon G, Narr KL, Poldrack RA, Bilder RM, Toga AW (2008) Construction of a 3D probabilistic atlas of human cortical structures. Neuroimage 39:1064–1080
22. Kingsbury AE, Bandopadhyay R, Silveira-Moriyama L, Ayling H, Kallis C, Sterlacci W, Maeir H, Poewe W, Lees AJ (2010) Brain stem pathology in Parkinson's disease: an evaluation of the Braak staging model. Mov Disord 25:2508–2515
23. Rochester L, Yarnall AJ, Baker MR, David RV, Lord S, Galna B, Burn DJ (2012) Cholinergic dysfunction contributes to gait disturbance in early Parkinson's disease. Brain 135:2779–2788

24. Emir UE, Tuite PJ, Oz G (2012) Elevated pontine and putamenal GABA levels in mild-moderate Parkinson disease detected by 7 tesla proton MRS. PLoS One 7:e30918
25. Baudrexel S, Nurnberger L, Rub U, Seifried C, Klein JC, Deller T, Steinmetz H, Deichmann R, Hilker R (2010) Quantitative mapping of T1 and T2* discloses nigral and brainstem pathology in early Parkinson's disease. Neuroimage 51:512–520
26. Scherfler C, Frauscher B, Schocke M, Iranzo A, Gschliesser V, Seppi K, Santamaria J, Tolosa E, Hogl B, Poewe W (2011) White and gray matter abnormalities in idiopathic rapid eye movement sleep behavior disorder: a diffusion-tensor imaging and voxel-based morphometry study. Ann Neurol 69:400–407
27. Tuite PJ, Mangia S, Tyan AE, Lee MK, Garwood M, Michaeli S (2012) Magnetization transfer and adiabatic R1rho MRI in the brainstem of Parkinson's disease. Parkinsonism Relat Disord 18:623–625
28. Zaccai J, Brayne C, McKeith I, Matthews F, Ince PG (2008) Patterns and stages of alpha-synucleinopathy: relevance in a population-based cohort. Neurology 70:1042–1048
29. Kalaitzakis ME, Graeber MB, Gentleman SM, Pearce RK (2008) The dorsal motor nucleus of the vagus is not an obligatory trigger site of Parkinson's disease: a critical analysis of alpha-synuclein staging. Neuropathol Appl Neurobiol 34:284–295
30. Parkkinen L, Pirttila T, Alafuzoff I (2008) Applicability of current staging/categorization of alpha-synuclein pathology and their clinical relevance. Acta Neuropathol 115:399–407
31. Halliday GM, Del Tredici K, Braak H (2006) Critical appraisal of brain pathology staging related to presymptomatic and symptomatic cases of sporadic Parkinson's disease. J Neural Transm Suppl 70:99–103